Combustion reaction kinetics of char from in-situ or ex-situ pyrolysis of oil shale

Rongxuan Linghu[a], Yuming Zhang[a]*, Mengxuan Zhao[a],
Lei Huang[a], Guogang Sun[a], Shu Zhang[b]*

[a] State Key Laboratory of Heavy Oil Processing, China University of Petroleum-Beijing, Beijing 102249, P.R. China
[b] College of Materials Science and Engineering, Nanjing Forestry University, Nanjing 210037, Jiangsu, P.R. China

Abstract. *Char produced from the oil shale retorting process represents a significant environmental hazard and causes the waste of the resource due to its residual contents of aromatics and unconverted carbon. As an important step of oil shale retorting technology, the combustion of char can make full use of its heat value and the ash generated could be used as a solid heat carrier to favour oil shale pyrolysis. The reaction kinetics of char combustion was studied using a thermal gravimetric analyzer (TGA) under minimized internal and external diffusion conditions by applying the isoconversional method. It was found that the average activation energy (E_a) of ex-situ char combustion was about 40.84 kJ/mol in the temperature range of 750–870 °C. The experimental char combustion data was fitted with different reaction models for its reaction mechanisms. A 3D nucleation and nuclei growth model had a good fitting coefficient of $R^2 > 0.99$ due to its assumed similarity to that of the real char combustion process. Combustion of char using different oxygen concentrations was investigated. The process E_a increased by about 20% when oxygen concentration was increased from 5 to 10%. Finally, combustion of in-situ char, i.e. hot char directly from pyrolysis, was compared with that of ex-situ (cold) char. The results showed that the E_a of in-situ char combustion was significantly reduced, by 32%, being even lower than the E_a of ex-situ char combustion using 20% oxygen.*

Keywords: *oil shale pyrolysis, char combustion, kinetic model, activation energy.*

1. Introduction

Char, as the by-product of oil shale retorting, is a potentially harmful solid waste because it contains toxic organic components and heavy metals [1–3]. In fact, the organic compounds remaining in char would be potentially combusted for heat, and thus char could be considered as a carbonaceous solid fuel and

* Corresponding authors: e-mails *ymzhcup@163.com*; *s.zhang@njfu.edu.cn*

used for combustion [4–5]. The recommended processing approach to deal with low calorific char in an environmental-friendly way is co-combustion with high calorific fuels in a circulating fluidized bed (CFB) combustor [6–7]. However, for co-combustion the heating value of the blended fuel is usually required to be high enough, 5000 kJ/kg, which, however, leads to high treatment cost. Consequently, the direct combustion of char is desirable to cause less harm to the environment and ensure an efficient resource utilization and energy recovery [8]. Many experiments on pyrolysis of oil shale have been performed, showing that the devolatilization of oil shale mainly occurs in the temperature range of 400–600 °C [9–11]. Therefore, this paper uses the char produced by the pyrolysis of oil shale at 600 °C for the subsequent combustion tests.

On the basis of the retorting technology process and the characteristics of oil shale, Han et al. [12] recommended a combined system with a fluidized bed (FB) reactor for retorting oil shale and a circulating fluidized bed boiler for burning char and fuel gases, to realize an efficient and clean use of oil shale. The hot char from FB will be conveyed directly to the CFB combustor as a fuel. This use of char is herein called "in-situ char" combustion. In the UTT-300 or Enefit280 technology, the ash produced by char combustion would continue to be used as a solid heat carrier and mixed with raw oil shale to provide the necessary heat for the pyrolysis reaction, thus greatly improving the energy utilization efficiency of the entire process [13, 14]. However, limited by factors such as processing capacity and cycle ratio, not all char would be burned in situ or completely. As a result, part of it will be removed from the combustor and subjected to further processing, which is herein called "ex-situ char" combustion. The differences between the in-situ and ex-situ char combustions are also considered in this paper.

Until now, the research on oil shale char combustion has been mainly based on the non-isothermal or co-combustion experiments with other high calorific value fuels, while the isothermal combustion experiments with merely oil shale char have been seldom considered. The isothermal reaction characteristics of char combustion were often tested in a real gasifier or combustor for the design and operation purpose. Miao et al. [15] have produced char from Daqing oil shale at 600 °C and studied its non-isothermal combustion characteristics. The results showed that the ignition temperature and the burnout temperature of the char were about 337 °C and 650 °C, respectively. For isothermal combustion, the temperature was set to a higher degree than the burnout temperature in non-isothermal combustion. Qin et al. [16] researched the thermal behavior of Longkou oil shale char and furfural residue, and their blends. According to the investigators, the char combustion process could be divided into two stages: thermal decomposition of volatile (360–655 °C) and fixed carbon burnout (655–810 °C). An nth-order reaction model with the model function f(X) = $(1-\alpha)^n$ was used to perform the kinetic analysis of the experimental results. The study of the co-combustion process kinetics showed that blending with

furfural residue could promote the char combustion, and the co-combustion of blends was a complicated process. Yang et al. [17] investigated the co-combustion behavior of Fushun low calorific oil shale and its char by using thermogravimetric analysis (TGA). The results showed that the addition of oil shale had a relatively slight positive effect on the ignition of the sample, but greatly improved the combustion intensity, combustion stability and burnout of the samples. The Coats-Redfern method and the nth-order reaction model were employed to calculate the activation energy (E_a) based on the experimental results.

In this paper, different models, such as a 3D nucleation and nuclei growth model, were applied to fit the experimental data and to describe the progress of the entire reaction process. Based on the data fitting using various kinetic models, this paper innovatively proposes a mechanism and process description for the isothermal combustion reaction of oil shale char. It lays a foundation for the design of a suitable reactor and the industrial utilization of oil shale char combustion.

2. Experimental

2.1. Materials

The char samples were produced from Huadian oil shale, Jilin Province, China. The oil shale was pyrolyzed in a fixed bed in a nitrogen atmosphere at 600 °C, to obtain the char samples. Prior to the experiment, the char samples were crushed and sieved to the desired sizes and dried at 105 °C for 3 h. The results of proximate and ultimate analyses of Huadian oil shale and its char are presented in Table 1. The oil shale char contains a high amount of ash and a relatively low amount of carbon, so it is often discarded as waste. As a result, the char might be harmful to the environment because it contains a considerable amount of toxic volatile matter.

Table 1. Proximate and ultimate analyses and heat values of Huadian oil shale and char

Sample	Proximate analysis, wt%, ad				Ultimate analysis, wt%, db					$Q_{ar,net}/$ (kJ/kg)
	A	V	FC	M	C	H	O*	N	S	
Oil shale	69.80	24.57	3.80	1.83	13.90	1.73	11.83	0.37	0.54	9517.9
Oil shale char	74.86	15.91	7.91	1.32	13.58	0.75	7.99	0.54	0.96	3517.0

* By difference.

2.2. Experimental procedures

The experiments were performed in a thermogravimetric analyzer TGA/ DSC 6300 (SETARAM Inc., France). The isothermal char combustion experiments were carried out in the temperature range of 750–870 °C. The char sample, loaded in advance into the alumina crucible, was heated from 30 °C to the pre-set reaction temperature at 30 °C/min under N_2 atmosphere. After the temperature was steady, the char combustion reaction was initiated by switching the gas into TGA from N_2 to $N_2 + O_2$. The reaction lasted until the weight loss of the sample was stabilized. Each experiment was repeated at least twice to ensure the repeatability and accuracy of the data.

3. Results and discussion

3.1. Measurement and reaction conditions determination

Figure 1 shows a typical reaction process in TGA and the combustion stage of char can be easily determined from the presented TG and DTG curves. The zero point of the time axis in the figure was the time point at which the gas was switched. It should be pointed out that, unlike non-isothermal char combustion, there is no obvious "double peak" or "three peaks" in the DTG curve of isothermal combustion [18–20]. The isothermal combustion is a process that involves many parallel reactions, so there is only one apparent weight loss peak in the DTG curve.
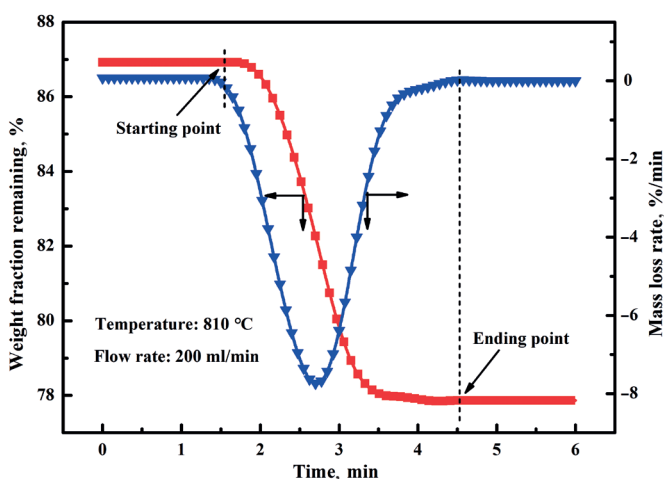

Fig. 1. Reaction behavior of ex-situ char combustion at 20% oxygen and 810 °C.

To find suitable conditions that could minimize the inhibition of external and internal diffusion of measurement in TGA, a series of tests were conducted at 750 °C by varying the initial mass of the char samples from 0.29 to 10.77 mg,

the flow rate of the gases from 50 to 200 ml/min and the diameter of the char particles from 0.074 to 1 mm. It needs to be pointed out that the specific surface area of char was only 1 m²/g from BET analysis. As a result, the internal diffusion effects could be suppressed to a maximum extent during the char combustion because of its small specific surface area. From Figure 2a–c it can be seen that carbon conversion vs char combustion reaction time changed little under the conditions of 0.6 mg sample amount, 200 ml/min gas flow rate and < 0.2 mm char particle size, which indicated low external diffusion effects [21]. Thus, the above conditions were applied in the subsequent experiments on the reaction kinetics of char combustion.
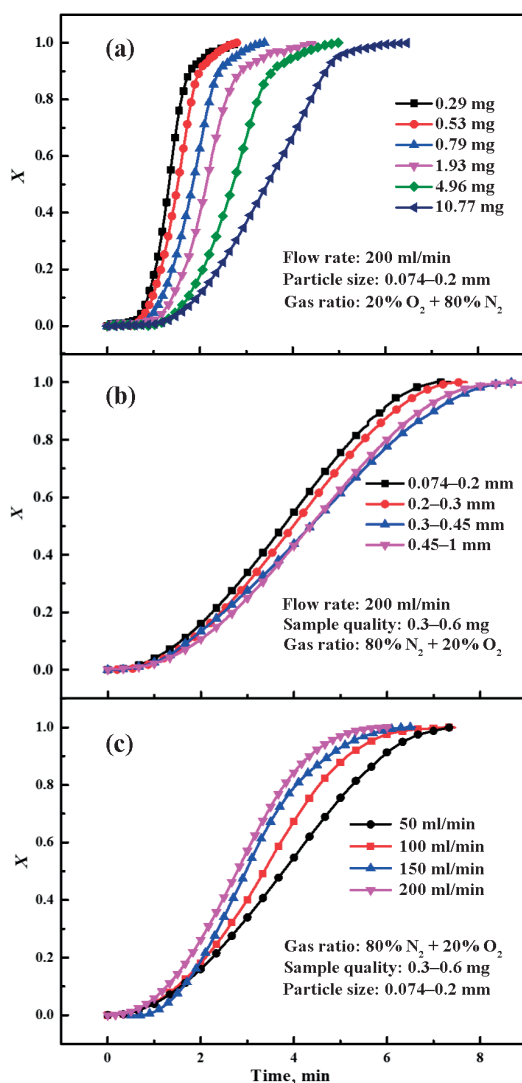

Fig. 2. Effect of various operating conditions on char combustion in air: (a) char sample amount, (b) char particle size, (c) gas flow rate.

3.2. Study of char combustion kinetics by the isoconversional method

Figure 3 correlates the carbon conversion *X* and reaction time *t* for cold char (i.e. ex-situ char samples) with 20% O_2 combustion (similar to air composition) at different temperatures under the minimized diffusion conditions. Being a process with significant heat release, the oil shale char combustion is highly affected by temperature. The char combustion reaction rate in the low-temperature range (≤ 810 ℃) was low with the relatively long time required to reach the same conversion ratio, while the reaction rate considerably increased with increasing temperature. In the higher temperature range (≥ 840 ℃) the reaction rate increased but little with increasing temperature [22] due to the relatively high reaction rate of char combustion.
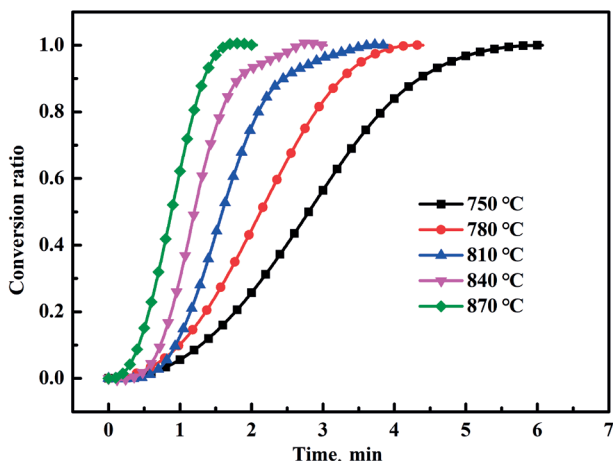

Fig. 3. Carbon conversion vs reaction time of ex-situ char combustion at different reaction temperatures.

Figure 4 shows the relationship between the reaction rate and carbon conversion for char combustion in air. The reaction rate was high when the carbon conversion was 0.2–0.7 at all the studied temperatures, indicating that the char structure would be changed as the reaction progressed. Figure 4 also shows the BET surface area and pore volume of oil shale char as a function of conversion at 750 °C. At the beginning of the reaction, the pore structure became more developed and thus the reaction rate gradually increased. When the reaction approached the end, the fixed carbon was almost exhausted and the developed pore structure was destroyed by the thermal stress, thus leading to the gradually reduced reaction rate.
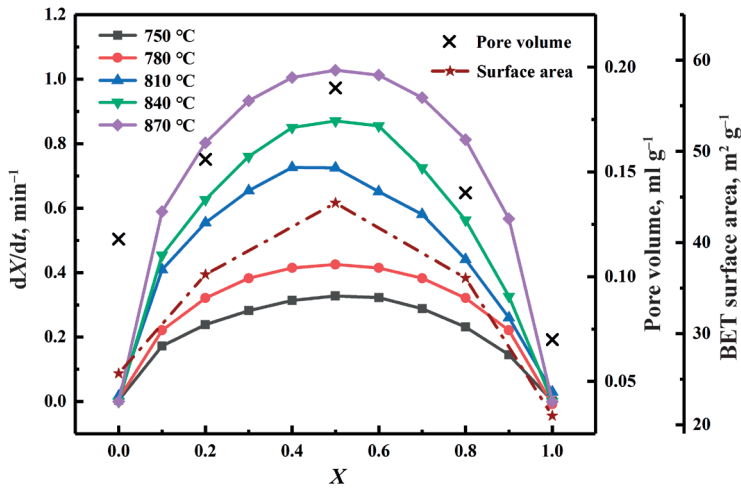
Fig. 4. Char combustion reaction rate vs carbon conversion at different reaction temperatures and the relationship between pore structure and conversion at 750 °C.

The analysis of the gas-solid reaction kinetics was usually based on a single-step kinetics, as shown by Equation (1):

$$\frac{dX}{dt} = k(T)f(X),$$ (1)

where t represents the time, T represents the temperature, X represents the conversion ratio, and $f(X)$ is the reaction model. The expression of X and dX/dt is shown in Equations (2) and (3), respectively:

$$X_i = \frac{W_0 - W_i}{W_0 - W_{ash}} \times 100\%,$$ (2)

$$\frac{dX_i}{dt} = -\frac{1}{W_0 - W_{ash}} \frac{dW_i}{dt},$$ (3)

where W_0, W_i and W_{ash} represent the initial mass, the instantaneous mass and the ash mass of the sample, respectively. The rate constant $k(T)$ is expressed as an Arrhenius-type temperature dependence:

$$k = A_{exp}(-E_a / RT).$$ (4)

Substituting Equation (4) into Equation (1) and taking the logarithm of both sides of the equation, we get:

$$\ln\left(\frac{dX}{dt}\right) = \ln A - \frac{E}{RT} + \ln f(X), \qquad (5)$$

where dX/dt is the reaction rate at a fixed carbon conversion, R is the universal gas constant and T stands for different isothermal temperatures. In this case, the model-free isoconversional method is recommended as an effective approximation by the ICTAC Kinetics Committee for the calculation of activation energy [23]. According to Equation (5), $\ln(dX/dt)$ and $1/T$ must have a linear trend when the experimental data are ideally simulated. The activation energy (E_a) can be obtained from the slope of the straight. Figure 5 shows the fitting results and Table 2 lists the values of kinetic parameters. The linear coefficient R^2 with respect to the value of $\ln(dX/dt)$ and $1/T$ was higher than 0.98 for each conversion ratio from 0.2 to 0.9 in Figure 5. The corresponding average E_a value within the above range was 40.84 kJ/mol (Table 2).
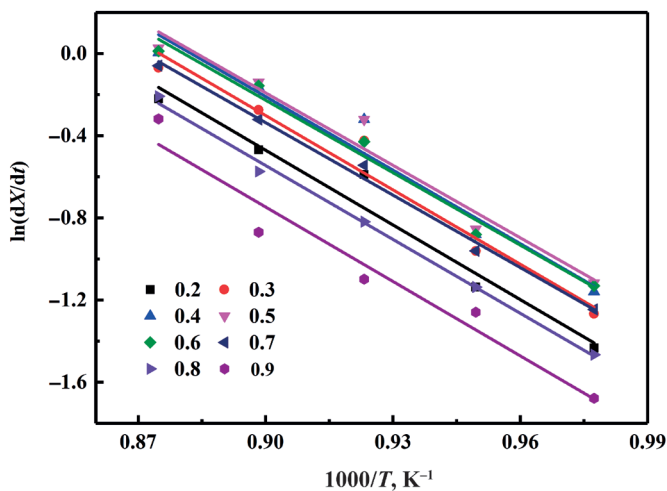

Fig. 5. Logarithm of the reaction rate vs $1/T$ at different conversion ratios during the ex-situ char combustion in air.

Table 2. Kinetic data of ex-situ char combustion at 20% oxygen

Conversion ratio	Linear fitting equation	R^2	E_a, kJ/mol	Average E_a, kJ/mol
0.2	Y = –4808.05X + 4.627	0.983	39.97	
0.3	Y = –4872.87X + 4.859	0.981	40.51	
0.4	Y = –5002.90X + 5.104	0.991	41.59	
0.5	Y = –5055.85X + 5.180	0.996	42.03	
0.6	Y = –4929.47X + 4.948	0.989	40.98	40.84
0.7	Y = –4841.27X + 4.687	0.991	40.25	
0.8	Y = –4919.45X + 4.515	0.984	40.90	
0.9	Y = –4867.21X + 4.762	0.990	40.47	

3.3. Determination of the model mechanism function

After the determination of activation energy using the isoconversional method, a model fitting process was applied to find the model function g(X), which could better describe the isothermal combustion process. The g(X) is the integral form of f(X), as shown in Equation (6):

$$g(X) = \int_0^X \frac{1}{f(X)}\, dX. \tag{6}$$

Combining Equations (1) and (6), the integral shift term of Equation (1) can be used to obtain Equation (7):

$$g(X) = k(T)t. \tag{7}$$

Equation (7) was used to determine the most appropriate mechanism function g(X). According to the ICTAC Kinetics Committee [24], a database was created for the expressions of f(X) and g(X). Various expressions of g(X) can be found in the literature [24–27] and directly used for the determination of reaction kinetic models. Using g(X) values calculated at various conversion ratios derived from TGA tests, the linear coefficient R^2 between g(X) and t based on Equation (7) was obtained and is given in Table 3. Meanwhile, the kinetic parameters corresponding to each model function were obtained by the model-fitting approach.

Table 3. Linear coefficient R^2 with respect to g(X) and t

No.	Model	g(X)	Linear coefficient R^2	E_a, kJ/mol	Frequency factor, min^{-1}
1	Avrami-Erofeev (2D)	$[-\ln(1-X)]^{1/2}$	0.994	41.01	1.44
2	Avrami-Erofeev (3D)	$[-\ln(1-X)]^{1/3}$	0.998	40.84	9.58
3	Avrami-Erofeev (4D)	$[-\ln(1-X)]^{1/4}$	0.995	40.74	7.19
4	Diffusion (1D)	X^2	0.987	41.14	1.17
5	Diffusion (2D)	$(1-X)\ln(1-X) + X$	0.967	41.54	9.91
6	Diffusion (3D)	$[1-(1-X)^{1/3}]^2$	0.920	42.08	4.24
7	Ginstling-Brounshtein (4D)	$1-(2X/3)-(1-X)^{2/3}$	0.954	41.73	2.74
8	Power law (P4)	$X^{1/4}$	0.958	40.03	3.69
9	Power law(P3)	$X^{1/3}$	0.963	40.09	4.68
10	Power law(P2)	$X^{1/2}$	0.973	40.21	6.35
11	Zero-order (F0)	X	0.991	40.53	9.58
12	First-order (F1)	$-\ln(1-X)$	0.969	41.61	3.01
13	Second-order (F2)	$(1-X)^{-1}-1$	0.830	42.85	1.21
14	Third-order (F3)	$1/2[(1-X)^{-2}-1]$	0.648	44.11	6.04
15	Contacting sphere	$1-(1-X)^{1/3}$	0.991	41.22	6.68
16	Contacting cylinder	$1-(1-X)^{1/2}$	0.993	41.04	8.25

From Table 3 it can be seen that the values of R^2 were between 0.95 and 1.0 for most of the expressions of g(X) except for a few models (Table 3). In general, these models could be divided into three categories. The first category mainly included the Avrami-Erofeev model, the zero-order model, the contacting sphere model and the contacting cylinder model. The fitting coefficients of all the models were higher than 0.99, and the corresponding E_a values were very close to the E_a values obtained by the isoconversional method. The second category mainly included the diffusion (1D and 2D) model, the power law (P3 and P2) model and the first-order model. The fitting coefficients of these models were between 0.96 and 0.99. The fitting coefficients of all

the other models were below 0.96. It is worth noting that the Avrimi-Erofeev models 2D–4D presented a good linear relation between g(X) and t, while the 3D model exhibited the best linear relationship. These results suggested the applicability of the models to describing the oil shale char combustion, In addition, the E_a value obtained based on the Avrimi-Erofeev model was highly consistent with the results obtained by the isoconversional method, which further demonstrated the suitability of this model for describing the char isothermal combustion reaction process.

The combustion reaction processes of different fuels can usually be described using one or several specific models. The most commonly considered models are the first-order model, the contacting sphere model and the contacting cylinder model. Zhang et al. [28] investigated the regeneration kinetics and characteristics of spent fluid catalytic cracking (FCC) catalyst by using a micro-fluidized bed reactor analyzer (MFBRA). The investigators found that compared to the shrinking core model (SCM), the homogenous model (HM) better fitted to the reaction data. The homogeneous model, the first-order model in Table 3, proposed a hypothesis that the active sites were distributed evenly inside the solid particles, and the size of the particles remained unchanged in the reaction process, while only the particle density uniformly changed. The shrinking core model (the contacting sphere model in Table 3) assumed that the gasification reaction occurred only on the surface of spherical reactant particles, and the unreacted core would shrink gradually in the reaction process. The particle surface of the FCC catalyst was covered with a thin carbon layer. Since this layer was so thin, the particle size could be considered constant during the regeneration reaction. This was consistent with the assumption made by HM. However, SCM could suit better to describe the gasification reaction of petroleum coke in MFBRA than HM [29]. The tested petroleum coke had a high carbon content and contained almost no ash. In addition, it had very few pores and quite a low surface area. Thus the reactions between carbon and steam mainly occurred on the surface of the coke particle with its size gradually decreasing, which made the petroleum coke gasification process very similar to the one hypothesized by SCM.

The Avrami-Erofeev model has been widely used to describe phase transformations, including crystallization and reactions in the solid phase. Liang et al. [30] investigated the polymerization kinetics of two polymer blends via the Avrami-Erofeev equation, finding that as the exponent n in the equation changed, the three-dimensional microstructure of the polymer underwent the corresponding morphological change. Mei et al. [31] used the Avrami-Erofeev 3D model to describe the reduction of Fe_2O_3/Al_2O_3 by CO and demonstrated the formation and growth of Fe_3O_4 nuclei. Therefore, unlike SCM and HM, the Avrami-Erofeev 3D model tended to require a more complex three-dimensional structure of the solid particles for the gas-solid reaction. As a result, the material similar to that assumed by nucleation and nuclei growth must contain much ash to form a mineral skeleton, and only

then could it undergo a three-dimensional morphological change during the reaction. The proximate and ultimate analyses indicated that the oil shale char had a high content of ash and a low content of carbon. Therefore, based on model assumptions, the isothermal char combustion reaction mainly underwent the processes of nuclear formation and growth.

3.4. Char combustion under different conditions

In an actual industrial process, the oxygen concentration would change with the progress of char combustion in air and char burning might occur under oxygen deficient conditions. So it would not be reasonable to investigate the char combustion at a fixed concentration of oxygen. Considering this, the oil shale char combustion experiments were carried out using oxygen concentrations of 5 and 10%.

Figures 6a–b show respectively the relationship between char conversion ratio and time, and the logarithm value of reaction rate ($\ln(dX/dt)$) vs the reaction temperature reciprocal (1/T) during the isothermal char combustion in the temperature range of 750–870 °C at 10% oxygen. As can be seen from Figure 6a, the reaction rate was the lowest at 750 °C with the reaction time being about 6.5 min. The reaction rate was the highest at 870 °C, while the reaction time was about 3 min. The time span was quite short compared to other reactions. For the isothermal gasification of coal char in TGA, the reaction time increased from 3 minutes to 130 minutes as the temperature increased from 760 °C to 1000 °C [32]. Since the gasification reaction was a relatively slow process compared to the combustion reaction and was greatly affected by temperature, the change in reaction time was remarkable. For the isothermal combustion of biomass char in TGA, the reaction time increased from 18.8 minutes to 181 minutes as the temperature increased from 330 °C to 400 °C at a conversion ratio of 0.5 [33]. Biomass char was a high-carbon and low-ash fuel, so the effect of the reaction rate on the reaction time was significant. In summary, being a high-ash and low-carbon fuel, the time span of the isothermal combustion process of oil shale char should be very short, consistently with the experimental results of this paper. The short time span was a clear indication of the high reactivity of oil shale char, even under the spontaneous reaction conditions.

Table 4 presents the kinetic data for the combustion reaction at 750–870 °C calculated by the isoconversional and model-fitting methods. As the oxygen concentration decreased, the activation energy increased and the frequency factor decreased slightly. It indicates that at 10% oxygen, the char combustion rate was higher compared to that at 5% oxygen. The more frequently occurring effective collision means a stronger interaction between the char particles and O_2 molecules in TGA. The consistency of the kinetic results of the two methods further confirms the applicability of the Avrami-Eeofeev 3D model to the study of the combustion reaction of oil shale char.
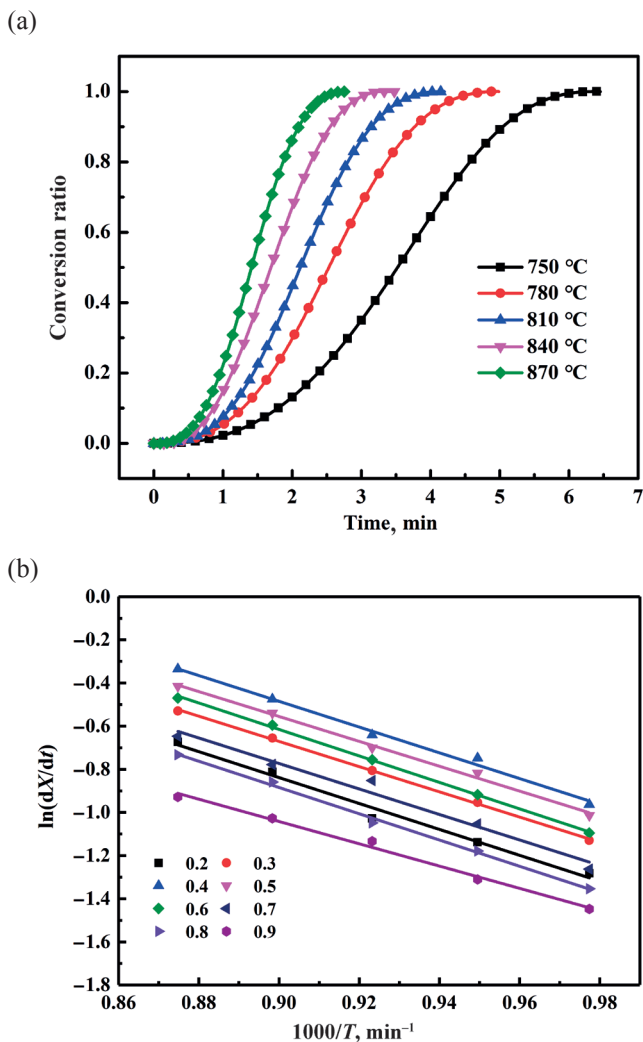
(a)

(b)

Fig. 6. Relationship between: (a) conversion ratio and time; (b) logarithm of the reaction rate and $1000/T$ at different conversion ratios at 10% oxygen.

Table 4. Kinetic data for ex-situ char combustion at 10% and 5% oxygen

Oxygen concentration	Isoconversional method		Model-fitting method	
	E_a, kJ/mol	Frequency factor, min^{-1}	E_a, kJ/mol	Frequency factor, min^{-1}
10%	48.72	118.0	48.36	788.0
5%	49.67	105.0	49.01	28.0

3.5. Comparison of the kinetics of in-situ and ex-situ char combustion

The char generated by pyrolysis of oil shale can be burned after cooling or directly reacted at a higher temperature in the combustor for some combined process [34, 35]. The char obtained after cooling in the reactor was called herein ex-situ char. During the cooling process, the pore structure and functional groups would change, and the combustion activity of ex-situ char was inevitably affected. The in-situ char referred to herein as hot char in the reactor was directly subjected to combustion without cooling, and the pore structure was not destroyed by the cooling process. Generally, the combustion activity of in-situ feedstock could be higher than that of the ex-situ materials [32, 36]. It was essential to fully understand the difference between in-situ and ex-situ char combustion characteristics because both char samples could be used in practical industrial applications for process design. Since char combustion might be actually carried out in oxygen-deficient conditions, the 5% oxygen was used to investigate the combustion kinetics of in-situ char (Table 5) and ex-situ char (Table 4).

Table 5. Kinetic data for in-situ char combustion at 5% oxygen

Conversion rate	Linear fitting equation	R^2	Average E_a, kJ/mol	Frequency factor, min^{-1}
0.2	Y = –3902.26X + 5.220	0.915		
0.3	Y = –4129.38X + 5.505	0.999		
0.4	Y = –4146.41X + 4.503	0.999		
0.5	Y = –4119.61X + 5.378	0.986	33.85	159.0
0.6	Y = –3858.32X + 5.048	0.968		
0.7	Y = –4083.47X + 5.213	0.993		
0.8	Y = –4203.82X + 4.295	0.931		
0.9	Y = –4125.29X + 5.188	0.996		

Figure 7 shows comparatively the E_a values of oil shale char combustion under different reaction conditions. In the figure, the straight line represents the average value of E_a at different conversion ratios. The results show that as the oxygen concentration decreased, the E_a of ex-situ char combustion increased gradually. When the oxygen concentration decreased to 5%, the E_a was increased by nearly 22%. This shows that oxygen concentration had a significant effect on the char combustion process. In practical industrial installations, the air was generally used as the reaction agent. When the air intake was insufficient, partial combustion of char would occur under anoxic

conditions, resulting in incomplete combustion. Therefore, maintaining sufficient air circulation helped to reduce the E_a of the combustion reaction and increased the combustion reactivity of the char [17].
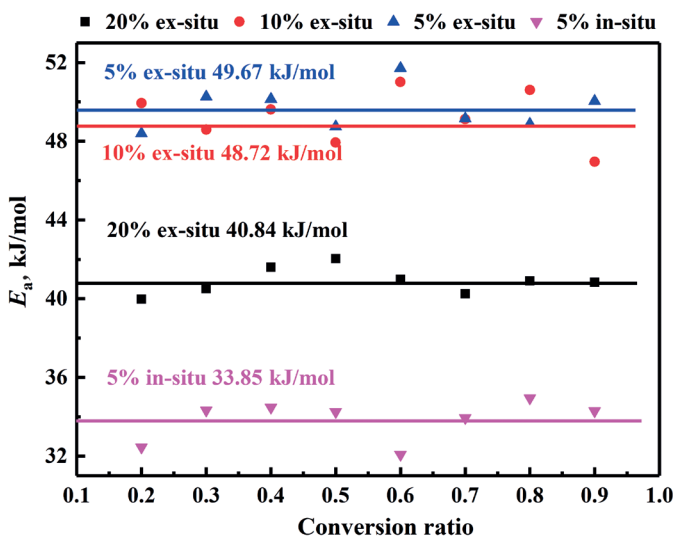

Fig. 7. Comparison of E_a values under different combustion reaction conditions.

Compared with the ex-situ char combustion at 5% oxygen, the E_a of in-situ char combustion was greatly reduced, by 32%, being even lower than the E_a of ex-situ char combustion at 20% oxygen. The reason was that although oil shale char contained less carbon, the vacant mineral skeleton and pore structure after sufficient pyrolysis provided an excellent environment for the diffusion and adsorption of oxygen, making the reaction activation energy decrease significantly. In contrast, the pore structure of rapidly-cooling char would inevitably collapse or get blocked, and the combustion reactivity was thus reduced [36].

4. Conclusions

The kinetics of char isothermal combustion was investigated using a thermogravimetric analyzer under minimized inhibition of external and internal diffusion. A series of isothermal combustion experiments were first carried out using 20% oxygen mixed with nitrogen, i.e. similar to air. The activation energy of the reaction was 40.84 kJ/mol according to the isoconversional method. Based on the fitting of experimental data with different kinetic models, the Avrami-Erofeev 3D model was proved to be a suitable model to describe the reaction process. When the oxygen concentration was reduced

from 20 to 5%, the char combustion activation energy was reduced by nearly 18%. This indicated that the oxygen concentration had a significant effect on the char combustion process.

For the industrial process, the char generated by pyrolysis of oil shale could be directly subjected to further treatment without cooling, as in-situ char. The activation energy of in-situ char combustion under 5% oxygen atmosphere was significantly reduced, by 32%, unlike that of ex-situ char combustion. It fully demonstrated that the in-situ char with developed pore structure and superior reaction environment could promote the char combustion reaction process. In summary, the in-situ char combustion under oxygen-rich conditions could improve its reaction properties, thus providing new ideas for the industrial utilization of char.

Acknowledgments

REFERENCES

1. Han, X., Jiang, X., Cui, Z., Liu, J., Yan, J. Effects of retorting factors on combustion properties of shale char. 3. Distribution of residual organic matters. *J. Hazard. Mater*., 2010, **175**(1−3), 445−451.
2. Külaots, I., Goldfarb, J. L., Suuberg, E. M. Characterization of Chinese, American and Estonian oil shale semicokes and their sorptive potential. *Fuel*, 2010, **89**(11), 3300−3306.
3. Datangel, B., Goldfarb, J. L. Heavy metals in Colorado and Chinese oil shale semicoke: disposal issues, impediments to byproduct conversion. *Energ. Fuel.*, 2011, **25**(8), 3522−3529.
4. Dung, N. V. Factors affecting product yields and oil quality during retorting of Stuart oil shale with recycled shale: a screening study. *Fuel*, 1995, **74**(4), 623−627.
5. Dung, N. V. Yields and chemical characteristics of products from fluidized bed steam retorting of Condor and Stuart oil shales: effect of pyrolysis temperature. *Fuel*, 1990, **69**(3), 368−376.
6. Wang, Z., Deng, S., Gu, Q., Zhang, Y., Cui, X., Wang, H. Pyrolysis kinetics study of Huadian oil shale, spent oil shale and their mixtures by thermogravimetric analysis. *Fuel Process. Technol.*, 2013, **110**, 103−108.
7. Liu, H., Liang, W. X., Qin, H., Wang, Q. Synergy in co-combustion of oil shale

semi-coke with torrefied cornstalk. *Appl. Therm. Eng.*, 2016, **109**(Part A), 653−662.

8. Han, X., Kulaots, I., Jiang, X., Suuberg, E. M. Review of oil shale semicoke and its combustion utilization. *Fuel*, 2014, **126**, 143−161.

9. Jiang, X., Han, X., Cui, Z. Mechanism and mathematical model of Huadian oil shale pyrolysis. *J. Therm. Anal. Calorim.*, 2006, **86**(2), 457−462.

10. Williams, P. T., Ahmad, N. Influence of process conditions on the pyrolysis of Pakistani oil shales. *Fuel*, 1999, **78**(6), 653−662.

11. Ma, Y., Li, S. The mechanism and kinetics of oil shale pyrolysis in the presence of water. *Carbon Resour. Convers.*, 2018, **1**(2), 160−164.

12. Han, X., Li, Q., Niu, M., Huang, Y., Jiang, X. Combined fluidized bed retorting and circulating fluidized bed combustion system of oil shale: 1. System and key issues. *Oil Shale*, 2014, **31**(1), 42−53.

13. Golubev, N. Solid oil shale heat carrier technology for oil shale retorting. *Oil Shale*, 2003, **20**(3S), 324−332.

14. Arro, H., Prikk, A., Pihu, T., Öpik, I. Utilization of semi-coke of Estonian shale oil industry. *Oil Shale*, 2002, **19**(2), 117−125.

15. Miao, Z., Wu, G., Li, P., Zhao, N., Wang, P., Meng, X. Combustion characteristics of Daqing oil shale and oil shale semi-cokes. *Mining Science and Technology*, 2009, **19**, 380−384.

16. Qin, H., Wang, W., Liu, H., Zhang, L., Wang, Q., Shi, C., Yao, K. Thermal behavior research for co-combustion of furfural residue and oil shale semi-coke. *Appl. Therm. Eng.*, 2017, **120**, 19−25.

17. Yang, Y., Lu, X., Wang, Q. Investigation on the co-combustion of low calorific oil shale and its semi-coke by using thermogravimetric analysis. *Energ. Convers. Manage.*, 2017, **136**, 99−107.

18. Wang, Q., Xu, H., Liu, H., Jia, C., Zhao, W. Co-combustion performance of oil shale semi-coke with corn stalk. *Energy Procedia*, 2012, **17**(Part A), 861−868.

19. Wang, Q., Sun, B., Wu, X., Bai, J., Sun, J. Study on combustion characteristics of mixtures of Huadian oil shale and semicoke. *Oil Shale*, 2007, **24**(2), 135−145.

20. Liu, H., Liang, W., Qin, H., Wang, Q. Thermal behavior of co-combustion of oil shale semi-coke with torrefied cornstalk. *Appl. Therm. Eng.*, 2016, **109**, 413−422.

21. Gómez-Barea, A., Ollero, P., Villanueva, A. Diffusional effects in CO_2 gasification experiments with single biomass char particles. 2. Theoretical predictions. *Energ. Fuel.*, 2006, **20**(5), 2211−2222.

22. Ollero, P., Serrera, A., Arjona, R., Alcantarilla, S. Diffusional effects in TGA gasification experiments for kinetic determination. *Fuel*, 2002, **81**(15), 1989−2000.

23. Vyazovkin, S., Wight, C. A. Model-free and model-fitting approaches to kinetic analysis of isothermal and nonisothermal data. *Thermochim. Acta*, 1999, **340−341**, 53−68.

24. Vyazovkin, S., Burnham, A. K., Criado, J. M., Pérez-Maqueda, L. A., Popescu, C., Sbirrazzuoli, N. ICTAC Kinetics Committee recommendations for performing kinetic computations on thermal analysis data. *Thermochim. Acta*, 2011, **520**(1−2), 1−19.

25. Arjmand, M., Keller, M., Leion, H., Mattisson, T., Lyngfelt, A. Oxygen release and oxidation rates of MgAl$_2$O$_4$-supported CuO oxygen carrier for chemical-looping combustion with oxygen uncoupling (CLOU). *Energ. Fuel.*, 2012, **26**(11), 6528−6539.

26. Song, H., Shah, K., Doroodchi, E., Wall, T., Moghtaderi, B. Analysis on chemical reaction kinetics of CuO/SiO$_2$ oxygen carriers for chemical looping air separation. *Energ. Fuel.*, 2014, **28**(1), 173−182.

27. Skrdla, P. J., Robertson, R. T. Dispersive kinetic models for isothermal solid-state conversions and their application to the thermal decomposition of oxacillin. *Thermochim. Acta*, 2007, **453**(1), 14−20.

28. Zhang, Y., Sun, G., Gao, S., Xu, G. Regeneration kinetics of spent FCC catalyst via coke gasification in a micro fluidized bed. *Procedia Eng.*, 2015, **102**, 1758−1765.

29. Zhang, Y., Yao, M., Gao, S., Sun, G., Xu, G. Reactivity and kinetics for steam gasification of petroleum coke blended with black liquor in a micro fluidized bed. *Appl. Energ.*, 2015, **160**, 820−828.

30. Liang, Y., Peng, H., Zhang, Y., Zhou, X., Liao, Y., Xie, X., Zhou, H. Relationship between polymerization kinetics and microstructure in reactive polymer blends: An Avrami-Erofeev study. *Eur. Polym. J.*, 2018, **106**, 72−78.

31. Mei, D., Zhao, H., Yan, S. Kinetics model for the reduction of Fe$_2$O$_3$/Al$_2$O$_3$ by CO in chemical looping combustion. *Chemical Engineering Processing: Process Intensification*, 2018, **124**, 137−146.

32. Zeng, X., Wang, F., Wang, Y., Li, A., Yu, J., Xu, G. Characterization of char gasification in a micro fluidized bed reaction analyzer. *Energ. Fuel.*, 2014, **28**(3), 1838−1845.

33. Morin, M., Pécate, S., Masi, E., Hémati, M. Kinetic study and modelling of char combustion in TGA in isothermal conditions. *Fuel*, 2017, **203**, 522−536.

34. Zhang, Y., Wang, Y., Cai, L., Yao, C., Gao, S., Li, C., Xu, G. Dual bed pyrolysis gasification of coal: Process analysis and pilot test. *Fuel*, 2013, **112**, 624−634.

35. Chen, Z., Li, Y., Lai, D., Geng, S., Zhou, Q., Gao, S., Xu, G. Coupling coal pyrolysis with char gasification in a multi-stage fluidized bed to co-produce high-quality tar and syngas. *Appl. Energ.*, 2018, **215**, 348−355.

36. Fang, Y., Luo, G., Li, J., Li, K., Chen, C., Zhao, H., Duan, R., Yao, H. Kinetic study on in-situ and cooling char combustion in a two-step reaction analyzer. *P. Combust. Inst.*, 2017, **36**(2), 2147−2154.